ORIGINAL PAPER

Spatial and temporal patterns of net nitrate uptake regulation and kinetics along the tap root of *Citrus aurantium*

Agostino Sorgonà · Giovanni Cacco ·
Lugi Di Dio · Wolfgang Schmidt ·
Paula Jay Perry · Maria Rosa Abenavoli

Abstract Spatial–temporal variation of the regulation and the kinetics of net nitrate (NO_3^-) uptake rate (NNUR) along the tap root of *Citrus aurantium* L. were analysed. Suberin incrustation in the peripheral cell layers and plasma membrane (PM) H^+-ATPase localisation, anatomical and physiological factors involved in NO_3^- uptake were also investigated. The results clearly indicated a spatially uniform distribution of the regulation process, accompanied by a temporal heterogeneous pattern of the kinetics of NO_3^- uptake along citrus tap root. In particular, kinetic analysis had a biphasic pattern, saturating (high affinity transport system) and linear (low affinity transport system), in response to increasing external NO_3^- concentrations in each root region, where 200 μM NO_3^- represented the threshold separating these two systems. Kinetic parameters, K_m and V_{max}, clearly indicated that apical segments reached the maximum value of induction before basal segments. Hence, the apical root zones, early exhibiting the maximum of potential capacity to absorb the NO_3^-, could be considered more efficient than basal root segments for acquiring NO_3^- from external solution. Suberin incrustations in the hypodermal cell layer, characterised by uniform fluorescence intensity among the root segments, could be responsible for the unchanged NNUR, while the PM H^+-ATPase could explain the temporal pattern of NNUR.

Keywords *Citrus aurantium* L. · *Citrus* rootstock · NO_3^- uptake · PM H^+-ATPase · Root exodermis

Introduction

To perform a variety of functions, the root system is composed of anatomically, morphologically and physiologically different root types, showing high plasticity with regard to the exploration of soil depth, the response to external signals, and the adaptation of the plant to heterogeneous nutrient supply (Waisel and Eshel 2002). The anatomical characteristics such as the occurrence of an exodermis located at different distances from the tip (Peterson 1988) and physiological functions, such as distinct respiratory rates (Mancuso and Boselli 2002) have been reported to vary along the root axis. These high anatomical and physiological complexities often determine the nutrient-specific absorption capacity over the root axis. For example, calcium uptake occurs in the apical region in barley (Mengel and Kirby 1980), sulphate is absorbed in the elongation zone immediately behind the meristematic zone (Holobrada 1977), while the phosphate influx appears to be a heterogeneous pattern along the root axis of basal bean roots (Rubio et al. 2004).

A high spatial variation of nitrate (NO_3^-) absorption has been found along the root axis in both annual and woody plants, although it is controversial. Indeed, the net flux of

Communicated by J. Zwiazek.

A. Sorgonà (✉) · L. Di Dio · M. R. Abenavoli
Dipartimento di Biotecnologie per il Monitoraggio
Agroalimentare ed Ambientale (BIOMAA),
Università degli Studi 'Mediterranea' di Reggio Calabria,
Salita Melissari, 89124 Reggio Calabria, Italy
e-mail: asorgona@unirc.it

G. Cacco
Dipartimento di Biotecnologie Agrarie, Università di Padova,
Viale dell'Università 16, 35020 Legnaro (PD), Italy

W. Schmidt · P. J. Perry
Institute of Plant and Microbial Biology, Academia Sinica,
Taipei, Taiwan, ROC

NO_3^- tended to be low near the root apex and increased towards the basal regions of maize (Henriksen et al. 1992) and barley roots (Siebrecht et al. 1995). In contrast for rice and carob seedlings decreasing NO_3^- fluxes with increasing distance from the root apex have been reported (Cruz et al. 1995; Colmer and Bloom 1998). Plassard et al. (2002) showed evidence that the highest NO_3^- uptake rates occurred at 20–50 mm of the root axis of *Pinus pinaster* and decreased at 60 mm from the root tip. More recently, Hawkins et al. (2008) demonstrated a marked spatial variability in ammonium (NH_4^+), NO_3^- and H^+ fluxes in roots of Douglas-fir and lodge pole pine.

No information on the regulation and kinetics of NO_3^- flux along the root axis is available. It is well known that NO_3^- uptake is a process highly regulated by high affinity transport system (HATS) activity, operating at low external NO_3^- concentrations (<200 μM), which consisted of constitutive HATS (cHATS) and induced HATS (iHATS) (Forde 2000). The cHATS, constitutively expressed in NO_3^--starved roots, mediates a constant NO_3^- uptake rate (Behl et al. 1988), while the iHATS is induced by NO_3^- and feedback regulated by downstream N metabolites (Forde 2000). Since NO_3^- was heterogeneously distributed in terms of time and space both in natural and management ecosystems (Caldwell 1994), quantitative information on the 'induction phase' could be useful to explain plant efficiency in capturing NO_3^- especially in N-limited soil. In this respect, the objective of the present study was to elucidate the spatial–temporal regulation of net nitrate (NO_3^-) uptake rate (NNUR) and the kinetic parameters along the tap root of citrus rootstock. Citrus is an interesting species due to the presence of anatomical root structures (Walker et al. 1984) such as the exodermis and suberin/lignin deposits, which could be responsible for different nutrient absorption capacity. For this purpose, transverse sections of citrus root segments corresponding to the zones of NO_3^- acquisition for suberin and lignin deposits were evaluated.

Further, since a close relation between NNUR and the PM H^+-ATPase activity (Santi et al. 1995, 2003) and H^+ flux (Garnett et al. 2003) was evident in the whole root system and also in specific regions of maize root (Monte et al. 2005), the localisation and the intensity of PM H^+-ATPase along the root axis of citrus tap root was also investigated.

Materials and methods

Plant cultivation

Citrus aurantium L. seeds, surface sterilised for 20 min in 20% sodium hypochlorite solution, were placed in aerated deionised water at 35°C for 2 days. Seeds were then transferred to germination paper moistened with 1 mM $CaSO_4$ in a growth chamber at 24°C and 70% relative humidity in darkness for 30 days. Thereafter, the seedlings, selected for uniform size, were transferred to 1 mM $CaSO_4$ solution and placed in the light with a 14-h photoperiod (300 μmol m^{-2} s^{-1} of photosynthetic photonic flux density, PPFD) in the same environmental conditions for a further 21 days. Nutrient solution pH was adjusted to 6.0 with 1 N KOH.

Net NO_3^- uptake assay

The NNUR was measured by the depletion method using a compartmented chamber (Engels et al. 2000) consisting of four compartments (each 2 cm × 2 cm). The intact tap root of 51-day-old citrus seedlings was placed in the chamber through a 3-mm wide hole in the side wall of each compartment, sealed with silicon. Four root regions were defined, according to the distance from the root apex: 0–2 (I), 2–4 (II), 4–6 (III) and 6–8 cm (IV). Before starting the experiments, the first and third compartments were filled with water to check for possible leaks.

Hence, each root region was washed three times for 10 min with nutrient solution containing 100 μM KH_2PO_4, 250 μM K_2SO_4 and 200 μM $MgSO_4$ to equilibrate the apoplast. Then, the root segments were exposed to the same aerated nutrient solution containing 100 μM KNO_3 for 0, 4, 8, 24, 32 and 48 h (induction period). At each induction period, the above nutrient solution was replaced with 1 mL of the same solution (uptake solution) and samples (100 μL) were taken at 30 min intervals over a 90 min period and the NO_3^- concentration was measured at 210 nm with a UV–Vis spectrophotometer (Perkin Elmer Lambda 35). The NNUR was calculated from the linear phase of the NO_3^- depletion curve on the basis of surface area (cm^2) and expressed as μmol NO_3^- $h^{-1}$$cm^{-2}$. During experiments, the compartmented chamber was covered with aluminium foil to keep tap roots in darkness, while shoots were illuminated at 300 μmol m^{-2} s^{-1} PPFD. Preliminary experiments were used to check the variation of the uptake solution volume during the 90 min of the experiment: the chamber was weighed at 0 and 90 min after the filling of the compartments with the uptake solution.

Kinetic parameters of net NO_3^- uptake

To determine the kinetics of net NO_3^--uptake, citrus seedlings were grown in the same experimental conditions as described above. Then, individual intact tap roots of seedlings (51 days old) were placed into a compartmented

chamber and each root region was exposed to continuously aerated nutrient solution complemented with 25, 50, 75, 100, 150, 200, 300, 500, 750 or 1,000 µM KNO_3 for 0, 4, 8 and 24 h (exposure period). For each exposure period and NO_3^- concentration, the above nutrient solution was renewed with 1 mL of the same solution (uptake solution) and samples (100 µL) were taken at 30 min intervals over a 90 min period and the NO_3^- concentration was measured at 210 nm with a UV–Vis spectrophotometer (Perkin Elmer Lambda 35). The NNUR was calculated as reported in the above paragraph.

H$^+$-ATPase immuno-cytolocalisation

Fixing, embedding and sectioning

To localise the PM H$^+$-ATPase protein by the immuno-detection technique, 51-day-old citrus seedlings, selected for uniform size, were transferred into a single growing unit containing 4.3 L of aerated nutrient solution supplemented with 100 µM KNO_3 for 24 h, which corresponded to the maximum of NNUR. Then, the tap root of the seedlings was cut into four root regions corresponding to 1–1.5, 3–3.5, 5–5.5 and 7–7.5 cm from the root apex. Each segment was fixed at 4°C in ethanol–acetic acid (3:1 v/v) for 24 h, dehydrated through a graded ethanol–tertiary-butanol series and embedded in paraffin (Paraplast plus, Sigma) at 60°C for 2–3 days. Serial sections of 6 µm were cut with a microtome (Leitz 1512, Germany), mounted on slides covered with gelatin (Gelatine Gold, Panreac), de-paraffinised in xylene and rehydrated through an ethanol series.

Immunolocalisation and quantification of PM H$^+$-ATPase protein

Immunological detection of PM H$^+$-ATPase protein in citrus root regions fixed as described above was performed according to Dell'Orto et al. (2002) with slight modifications. Sections were incubated for 30 min at room temperature in 5% H_2O_2, washed in water and subsequently in Tris buffer solution (TBS) (150 mM NaCl, 25 mM Tris–HCl, pH 7.6) for 20 min. Then, sections were incubated in TBS supplemented with 2% (w/v) bovine serum albumin (BSA) for 30 min at room temperature. Polyclonal antibody (IgG n. 759) raised against the C terminus of the *Arabidopsis thaliana* PM H$^+$-ATPase (kind gift by Dr. R. Serrano) was diluted 1:50 in TBS with 0.5% (w/v) BSA and incubated over-night at 4°C. After three washings for 5 min in TBS, root sections were incubated for 2 h at room temperature with a biotinylated second antibody (anti-rabbit IgG

biotin conjugate developed against goat, Sigma), diluted 1:1,000 in TBS with 0.5% (w/v) BSA. After three washings for 5 min in TBS, root sections were incubated in the ABC complex (Immuno Pure ABC Peroxidase Staining Kit-Standard-Pierce). After three washings of 5 min each in TBS, the peroxidase reaction was developed by incubation in acetate buffer pH 6.0 containing 0.01% (w/v) 3,3′ diaminobenzidine (DAB), 0.01% (v/v) H_2O_2 and 1.5% (w/v) $(NH_4)_2Ni(SO_4)_2 6H_2O$. This reaction produced a stable, insoluble brown precipitate which allowed for localisation of the H$^+$-ATPase protein. The intensity of immunoprecipitation was quantified using an image analysis system. Root section images were captured by a digital camera (Olympus U_CAMEDIA C-5050 ZOOM, Japan) and analysed by the software IMAGE PRO-PLUS 6.0 (MEDIA Cybernetics Inc.). The intensity was expressed as integrated optical density (IOD), where IOD = Optical density/total root area (µm^2).

Parallel sets of citrus root sections incubated with monoclonal anti-synaptobrevin (mouse IgG1, Sigma–Aldrich, Tokyo, Japan) that recognises the synaptic vesicle protein synaptobrevin (VAMP) in human and porcine tissue served as negative controls.

Root structure

Root structure of each root segment was investigated by light and fluorescence microscopy. For light microscopy analysis, root segments were fixed in 3.7% (w/v) paraformaldehyde in 100 mM phosphate buffer, pH 7.0, dehydrated in an increasing concentration ethanol series, infiltrated with London Resin White (London Resin Co. Ltd., London), and polymerised for 24 h at 55°C and 250 mbar. Cross sections (1 µm) were cut with a microtome (Ultracut E, Reichert, Vienna, Austria) stained with 0.05% (w/v) toluidine blue O for 1 min, and viewed in a dark field. Fluorescence microscopy investigations were carried out on transverse free-hand sections. To visualise suberisation of the epidermal and subepidermal cell walls, sections were stained with 0.1% (w/v) neutral red in 100 mM phosphate buffer, pH 6.0, for 1 min and washed twice with tap water. The specificity of the neutral red technique for the hydrophobic/lipid domain of suberin was shown previously (De Simone et al. 2003). For quenching of autofluorescence, sections were incubated for 2 h in 0.05% (w/v) toluidine blue O in 100 mM phosphate buffer, pH 6.0. Blue-violet excitation (exciter filter EX 420-490, dichromatic beamsplitter DM 505, barrier filter BA 520, Nikon, Tokyo, Japan) was used for all investigations of suberin deposits. Photographs were taken with a digital camera.

Calculations and statistical analysis

The experimental design was completely randomised, with five replicates. All data were checked for normality (Kolmogorov–Smirnov test) and tested for homogeneity (Leven Median test). Induction of the NNUR for each region of citrus tap root was described by non-linear regression. The following non-linear equation was applied:

$$I(t) = A - B \times \exp^{(-k \times t)} \tag{1}$$

where $I(t)$ is the NNUR (µmol NO_3^- h^{-1} cm^{-2}), A represents the maximum NNUR of the iHATS, and B is the NNUR of the cHATS both expressed as µmol NO_3^- h^{-1} cm^{-2}, k is the rate constant of the iHATS expressed in h^{-1}, and t is time in h. The $t_{1/2}$ (h), calculated from the ratio $Ln2/K_{ind}$, denotes the half time of NNUR of iHATS during the induction phase. The cumulative NO_3^- uptake over 24 h (A_t) was also calculated. The model parameters of the induction phase were estimated by the least squares method (TableCurve 2D v. 4.0 software, Jandel Scientific Ekrath, Germany) using the Levenberg–Marquardt optimisation algorithm. Non-linear regressions were repeated several times to minimise the sum of squares of deviation between predicted and experimental values to <0.01% between two consecutive fits (Press et al. 1992). The parameters relative to the induction phase of net NO_3^- uptake (A, B, $t_{1/2}$ and A_t) were tested by analysis of variance and Tukey's test was applied to compare the mean values of net NO_3^- uptake regulation parameters of different root segments ($P < 0.05$).

The kinetic analysis of net NO_3^- uptake (net NO_3^- uptake rate versus external NO_3^- concentrations) of each root segment was described by non-linear regression using the Michaelis–Menten equation:

$$v = V_{max} \times C/K_m + C \tag{2}$$

where v (µmol NO_3^- h^{-1} cm^{-2}) is the NNUR, V_{max} (µmol NO_3^- h^{-1} cm^{-2}) indicates the maximum NNUR, K_m is the concentration (µM) at which net NO_3^- uptake is half of V_{max} and represents the apparent affinity, and C is the external NO_3^- concentration. The kinetic parameters, V_{max} and K_m, were estimated by the least squares method as reported above. The effects of root segment, exposure time, and root-segment × exposure-time interaction on the kinetic parameters were tested by two-way ANOVA. Tukey's test was applied to compare the mean values of V_{max} and K_m parameters of different root regions for each time of exposure to NO_3^- ($P < 0.05$).

The effects of root segment, time of exposure, NO_3^- concentration and their interactions on IOD of H^+-ATPase immunostain were tested by three-way ANOVA. Tukey's test was applied to compare the mean values of IOD of H^+-ATPase immunostain of different root regions for each time of NO_3^- exposure ($P < 0.05$). All statistical analysis was conducted using the Systat 8.0 software package (SPSS Inc., Evanstone, IL, USA).

Results

Regulation and kinetics of net NO_3^- uptake

Upon initial contact with 100 µM NO_3^-, the NNUR immediately increased in all root regions of citrus seedlings (induction phase) and, at 24 h of exposure, reached complete induction (full induction) followed by an initial decay phase more evident in the I and II root regions (Fig. 1). The net NO_3^- uptake regulation parameters regarding the induction phase of NNUR, estimated by non-linear regression, did not vary along the tap root axis (Table 1).

The kinetic analysis revealed, in all root regions, a saturable uptake system (hyperbolic curve) operating at concentrations <200 µM NO_3^- (Fig. 2). At >200 µM, all root segments showed a linear curve except the I and II root segments, which exhibited a hyperbolic curve at 24 h of exposure (Fig. 2). The statistical parameters (R^2 and P values) obtained by fitting the hyperbolic and linear curves at 0–200 and >200 µM NO_3^-, confirmed the above results (Table 2).

Below 200 µM NO_3^-, the V_{max} did not vary significantly among the root regions at 0, 8 and 24 h of NO_3^- exposure (Fig. 3). Conversely, at 4 h of exposure, V_{max} increased differently in each root segment: the I segment was significantly higher than that of the IV (0.043 and 0.018 µmol NO_3^- $h^{-1}cm^{-2}$, respectively) while there were no significant differences between the II and III root segments (Fig. 3). Similar to V_{max}, the K_m did not vary significantly among the root regions at 0, 8 and 24 h of NO_3^- exposure; conversely, at 4 h there was a significant difference in K_m between the I and the more basal root segments (254 and 75 µM, respectively; Fig. 4).

Above 200 µM, with 24 h of NO_3^- exposure, V_{max} was 0.141 and 0.114 µmol NO_3^- h^{-1} cm^{-2} for the I and II root segments, respectively; K_m was 788 and 638 µM (data not shown).

H^+-ATPase immunolocalisation and quantification

The immunological localisation of PM H^+-ATPase was performed on four root sections of citrus seedlings after 24 h of exposure to 100 µM NO_3^-. Controls were

Fig. 1 Net NO_3^- uptake rate in different tap root segments (*I*, *II*, *III* and *IV*) of *Citrus aurantium* seedlings, 51 days old, exposed to 100 μM NO_3^-. Each *curve* represents the best fit on the experimental points using the non-linear equation as described in "Material and methods". R^2 and *P* are the statistical parameters of the non-linear regression fit
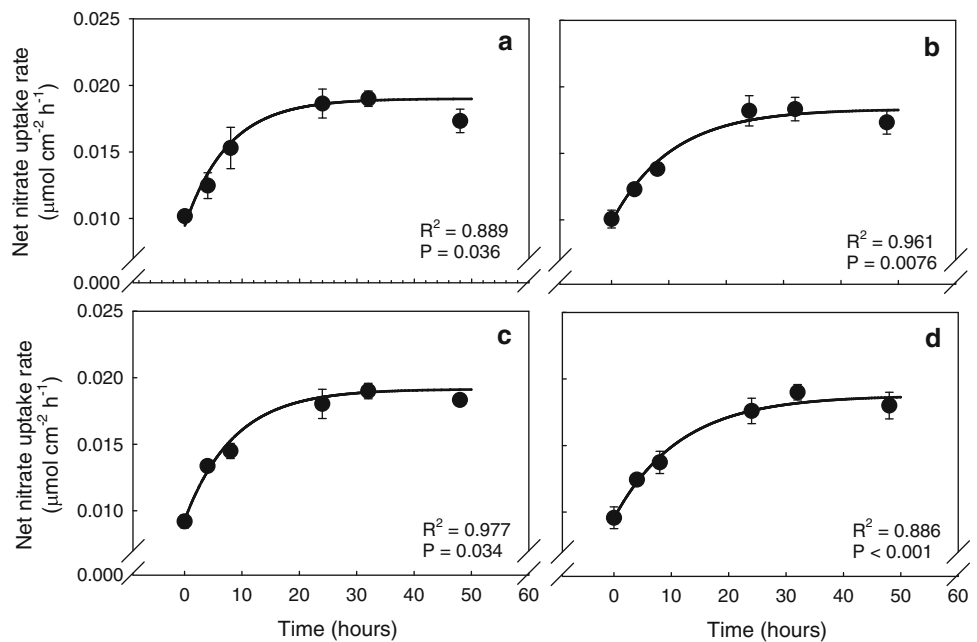

Table 1 Parameters relative to the net nitrate uptake regulation in different tap root segments of *Citrus aurantium*

	I segment	II segment	III segment	IV segment
A (μmol NO_3^- cm^{-2} h^{-1})	0.019 ± 0.0006[a]	0.0183 ± 0.0003[a]	0.0194 ± 0.0006[a]	0.0197 ± 0.0012[a]
B (μmol NO_3^- cm^{-2} h^{-1})	0.0095 ± 0.001[a]	0.0085 ± 0.0008[a]	0.0098 ± 0.0006[a]	0.0101 ± 0.001[a]
$t_{1/2}$ ind (h)	7.26 ± 2.76[a]	7.54 ± 0.94[a]	8.08 ± 3.41[a]	11.74 ± 4.7[a]
A_t (μmol NO_3^- cm^{-2})	0.813 ± 0.023[a]	0.789 ± 0.017[b]	0.815 ± 0.019[a]	0.780 ± 0.004[b]

The values into the brackets indicate the error standard. $N = 5$. Different letters along the rows indicated significant difference at $P = 0.05$ (Tukey's test)

A net nitrate uptake rate maximum of the inducible transport system, *B* net nitrate uptake rate of the constitutive transport system, $t_{1/2}$ the half time of the net nitrate uptake rate of the inducible transport system during the induction phase, A_t accumulated nitrate in 24 h [the parameters were estimated by the following non-linear equation $I(t) = A - B* \exp^{(-k* t)}$ (see "Materials and methods")]

performed with an unspecific monoclonal antibody anti-synaptobrevin.

The PM H^+-ATPase was clearly detectable in all segments of citrus tap root, from comparing roots treated with the specific H^+-ATPase antibody and different NO_3^- concentrations (0 and 100 μM NO_3^-). The specificity of the antibody reaction was verified by application of a non-specific antibody.

Tissue localisation indicated that ATPase protein was particularly concentrated in the endodermis, xylem and phloem tissues (Fig. 5). Furthermore, the immunodecoration decreased markedly towards more basal root regions (Fig. 5).

In the absence of NO_3^-, the IOD in the I root region was significantly higher than other segments, which all had similar IOD values. NO_3^- treatment caused a significant increase of IOD in all root regions compared to untreated ones; this increase was significantly higher in the I root region compared to the others, which had no significant difference in IOD values between them (Fig. 6).

Root structure

Non-specific autofluorescence in the four root sections, indicating both lignin and suberin deposits, is shown in micrographs (Fig. 7, left panel). Autofluorescence was restricted to the hypodermal cell layer without exhibiting major differences among the root segments investigated. Staining with the lipid cytofluorochrome neutral red, after quenching the autofluorescence of phenolic lignin and suberin components, allows for differentiation between lignin and suberin depositions in cell walls of the root epidermis (Lulai and Morgan 1992). The specificity of the staining method was proven by quantitative analysis of the composition of apoplasmic barriers in hypodermal cell walls by gas chromatography/
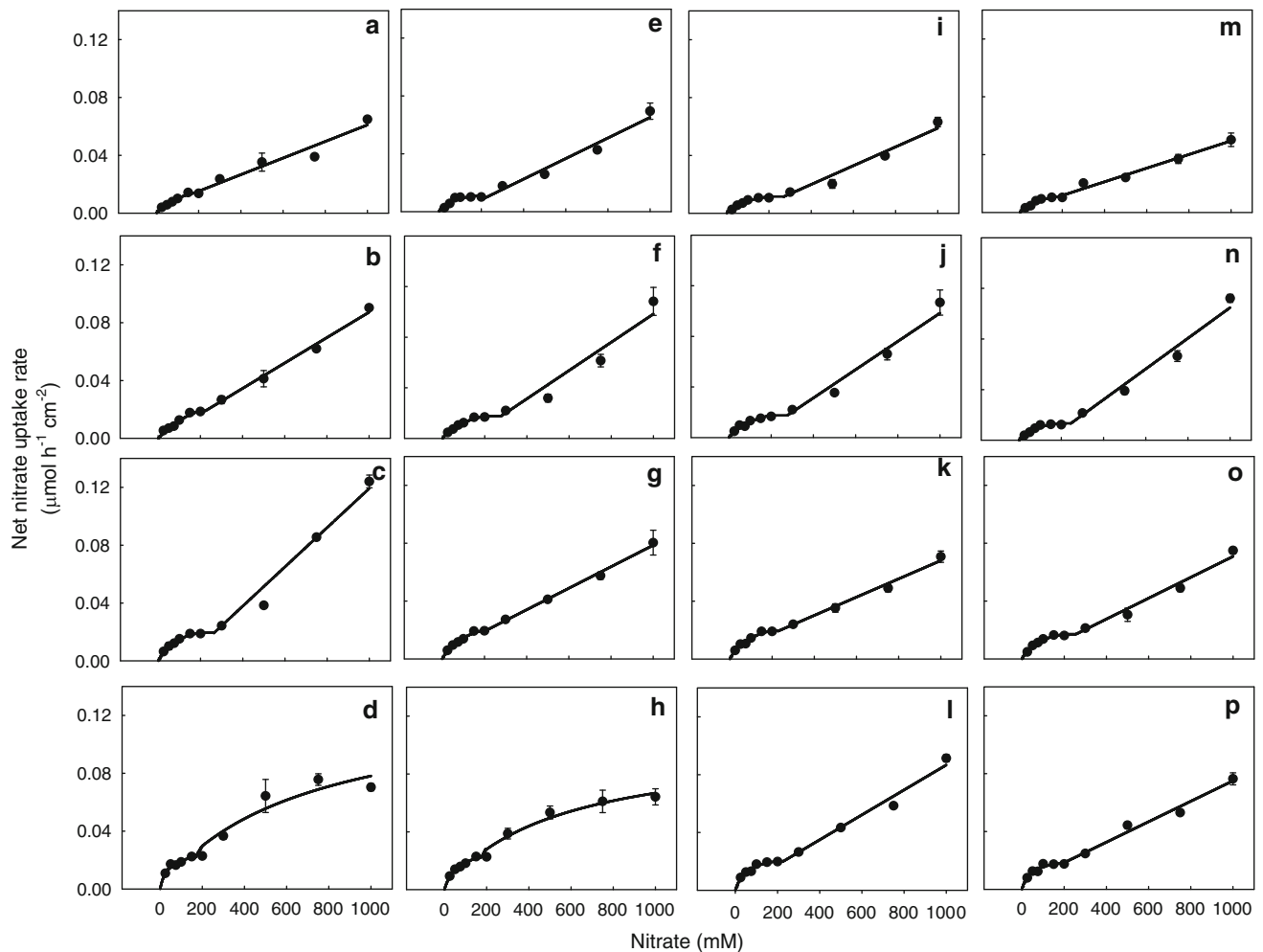
Fig. 2 Kinetics of the net NO_3^- uptake rate in different tap root segments (*I*, *II*, *III* and *IV*) of *Citrus aurantium* seedlings, 51 days old, at different times of NO_3^- exposure (0, 4, 8 and 24 h). **a–d** I segment at 0–24 h, **f–h** II segment at 0–24 h, **i–l** III segment at 0–24 h, **m–p** IV segment at 0–24 h. The statistical parameters of the regression analysis of each curve are reported in Table 2

mass spectrometry (De Simone et al. 2003). Epidermal cells were devoid of suberin deposits in all sections examined (Fig. 7, right panel). There were suberin incrustations in the hypodermal cell layer, without major differences in fluorescence intensity among the root segments, except in IV root section in which tangential cell walls of the hypodermis did not appear to contain suberin.

Discussion

Reliability and validity of depletion method

Citrus seedlings, intact and grown N-free, were used to measure NNUR along the tap root. The use of intact seedlings instead of root excision did not affect the shoot N-demand, which represented the driving force of NO_3^- uptake (Imsande and Touraine 1994) and did not reduce the assimilate allocation to the roots necessary for the NNUR, an energy-dependent process (Bloom and Caldwell 1988; Reidenbach and Horst 1997).

The use of N-starved seedlings allowed obtaining of better evidence of the 'induction phase' of NO_3^- uptake since, as well known, the NO_3^- uptake rate is positively correlated with root $[NO_3^-]$ (Siddiqi et al. 1989). Further, the use of N-starved seedlings and the exposure at low external NO_3^- level for measuring the NO_3^- uptake rate and kinetics (100 μM), made the contribution of efflux negligible, the second component of NNUR, and allowed the findings to be attributable only to the NO_3^- influx (Deane-Drummond and Glass 1983; Aslam et al. 1994; Gobert and Plassard 2002) which actually represented the mechanism up-regulation.

Table 2 Statistical parameters of the regression analysis obtained by fitting the hyperbolic and linear curves on 0–200 and >200 μM nitrate concentration ranges at 0, 4, 8 and 24 h of exposure

Time (h)	Curve type	Statistical parameters	I segment		II segment		III segment		IV segment	
			0–200 μM	>200 μM	0–200 μM	>200 μM	0–200 μM	>200 μM	0–200 μM	>200 μM
0	Linear	R^2	0.768	0.854	0.551	0.929	0.707	0.966	0.727	0.878
		F	52.9***	99.9***	27.0***	223.8***	38.6***	339.0***	58.7***	122.2***
	Saturable	R^2	0.840	0.849	0.774	0.906	0.859	0.954	0.867	0.875
		F	83.8***	95.3***	75.4***	164.0***	97.5***	251.7***	144.0***	119.6***
4	Linear	R^2	0.923	0.955	0.833	0.865	0.788	0.906	0.698	0.958
		F	264.0***	382.9***	110.1***	115.5***	81.7***	174.3***	48.6***	412.2***
	Saturable	R^2	0.929	0.954	0.888	0.833	0.834	0.879	0.876	0.913
		F	288.7***	377.5***	173.8***	90.0***	110.9***	130.7***	148.9***	188.8***
8	Linear	R^2	0.756	0.958	0.898	0.901	0.897	0.937	0.763	0.931
		F	68.1***	415.5***	193.4***	164.2***	191.4***	268.6***	70.7***	241.7***
	Saturable	R^2	0.825	0.922	0.939	0.897	0.943	0.927	0.886	0.930
		F	103.9***	213.6***	341.3***	157.1***	362.6***	229.6***	171.6***	238.7***
24	Linear	R^2	0.770	0.627	0.840	0.642	0.794	0.970	0.620	0.950
		F	73.9***	30.2***	115.4***	32.3***	84.9***	577.4***	35.9***	339.9***
	Saturable	R^2	0.851	0.722	0.914	0.723	0.881	0.968	0.776	0.949
		F	125.9***	46.9***	234.0***	47.1***	162.7***	561.9***	76.3***	334.7***

R^2 the coefficient of the determination, F the F value of the regression analysis
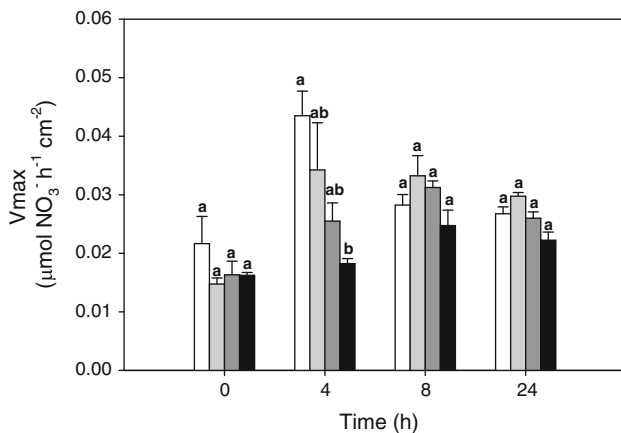
*** $P < 0.001$

Fig. 3 Spatial and temporal variation of V_{max} in different tap root segments [I (*white bar*), II (*light grey bar*), III (*dark grey bar*) and IV (*black bar*)] of *Citrus aurantium* (51 days old) exposed to NO_3^- for different times (0, 4, 8 and 24 h). *Different letters* indicate significant differences at $P < 0.05$ (Tukey's test)
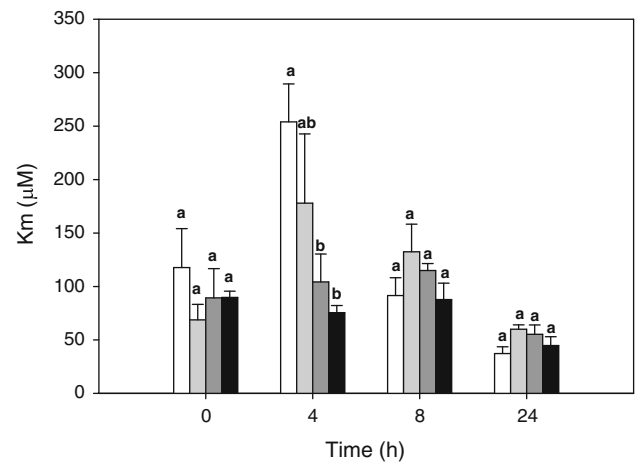

Fig. 4 Spatial and temporal variation of K_m in different root segments [I (*white bar*), II (*light grey bar*), III (*dark grey bar*) and IV (*black bar*)] of *Citrus aurantium* (51 days old) exposed to NO_3^- for different times (0, 4, 8 and 24 h). *Different letters* indicate significant differences at $P < 0.05$ (Tukey's test)

Spatial evolution of the regulation process and kinetics of NNUR

The regulation process of the NNUR along citrus tap root, reported here for the first time, was performed in each root region of citrus seedlings, showing an uniform distribution of NNUR. Indeed, the NO_3^- uptake rate increased (induction phase) reaching complete induction after 24 h of contact with the anion (full induction) in all root segments. This temporal pattern was similar to that reported for the whole root system of citrus seedlings (Sorgonà et al. 2005) and other woody species (Kronzucker et al. 1995; Gobert and Plassard 2002). An initial decay phase, characterised by a decline of the net NO_3^- uptake, was only observed in the more apical citrus root zones. This latter result contrasted with that observed in the whole root system of citrus
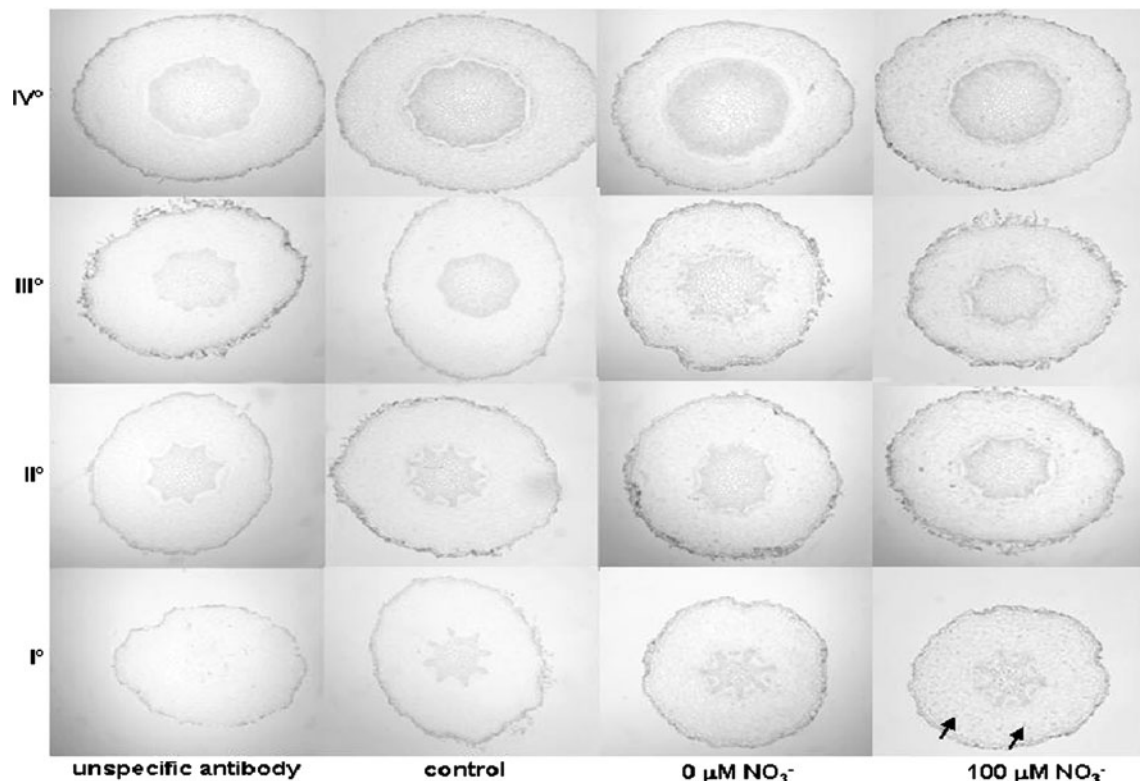
Fig. 5 Localisation of PM H$^+$-ATPase in cross sections of different tap root segments (*I, II, III* and *IV*) of *Citrus aurantium* (51 days old) exposed at 0 and 100 μM NO$_3^-$ for 24 h. Control indicated root section at time 0 h. *Arrows* showed the H$^+$-ATPase immunostain within the root cross sections
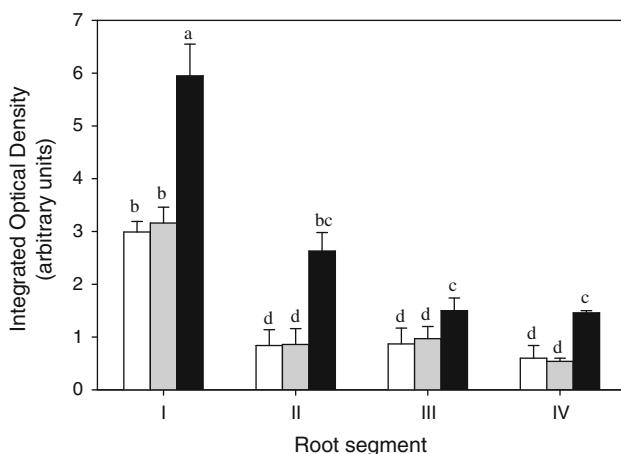

Fig. 6 Spatial variation of integrated optical density (IOD) of immunolocalisation of PM H$^+$-ATPase in different segments of tap root (*I, II, III* and *IV*) of *Citrus aurantium* seedlings (51 days old) exposed to 0 (*light grey bar*) and 100 μM NO$_3^-$ (*black bar*) for 24 h. The control is the immunolocalisation of PM H$^+$-ATPase at time 0 h (*white bar*). *Different letters* indicate significant differences at $P < 0.05$ (Tukey's test)

rootstocks where there was a clear decay phase after 48 h of NO$_3^-$ contact (Sorgonà and Cacco 2002; Sorgonà et al. 2005). Probably, a longer time of contact with NO$_3^-$ for
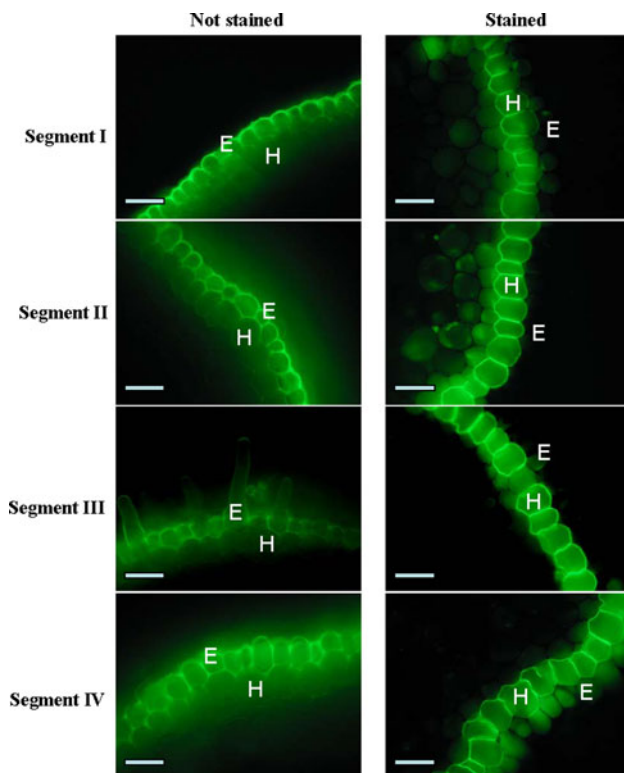
the root segment compared to whole root systems was needed to increase the N-status of plants and hence to determine the subsequent inhibition of NO$_3^-$ transport.

The spatial uniform distribution of NNUR was also confirmed by comparison of the regulation parameters of NNUR, which did not vary among tap root regions. Indeed, both components of the NNUR, cHATS (*B*) and iHATS (*A*), were similar in each root region. Further, the cHATS and iHATS values reflected that reported in whole root system of citrus rootstocks (Sorgonà et al. 2005) and for other plant species (Siddiqi et al. 1989). Although this spatial uniformity of NNUR was also reported by Colmer and Bloom (1998), Garnett et al. (2001) and Rubinigg et al. (2002), it contrasted with that reporting either an increase (Lazof et al. 1992; Colmer and Bloom 1998; Plassard et al. 2002) or a decrease of NO$_3^-$ fluxes from root tip (Cruz et al. 1995; Reidenbach and Horst 1997; Hawkins et al. 2008).

To resolve these contrasting results regarding the efficiency of the root segments in absorbing NO$_3^-$, the kinetic analysis which provides a measure of 'potential' capacity of the NO$_3^-$ transport system (unlike the NNUR that represents 'actual' capacity) was applied. The results indicated, for the first time, that in all root segments and times of exposure, the saturating Michaelis–Menten

Fig. 7 Autoflorescence of cross-section of tap root of *Citrus aurantium* stained with Blue-violet. *Scale* 0.03 mm. *Left panels* no stain, *right panels* stained, *E* epidermal cells, *H* hypodermal cells

kinetics occurred at external NO_3^- concentrations <200 μM, corresponding to the activity of the HATS; conversely, >200 μM NO_3^- the low affinity transport system (LATS) became apparent. Hence, 200 μM NO_3^- was a threshold concentration separating these two systems. This biphasic pattern (dual-phase) in response to increasing external NO_3^- concentrations was already reported in whole root systems of citrus seedlings by Cerezo et al. (1997) who, in contrast, indicated 1 mM NO_3^- was the threshold concentration between HATS and LATS systems. This contrasting result could be due to a different pattern of kinetics of NNUR at the time of maximum induction (24 h) between the apical/young (I and II) and basal/old root segments (III and IV) compared to the pattern of whole root systems obtained by Cerezo et al. (1997). A different old/young tissue ratio for the single root axis used in our experiment was probably responsible for the different NO_3^- threshold value.

However, the more interesting aspect of the present paper was related to the kinetic parameters which highlighted that the apical root zones were more NO_3^- uptake efficient than basal ones. Indeed, in the apical root segments (I and II), a double-saturation response to external NO_3^- concentration characterised by two different K_m values operating at ≤200 and 200–1,000 μM NO_3^-,

respectively, was observed. This pattern, also reported for whole root systems (Kronzucker et al. 1995), clearly indicated that segments closer to the root tip absorb NO_3^- more efficiently than basal segments. Further, this efficiency of apical root zones was confirmed by V_{max} that reached the maximum induction value at 4 h of exposure, compared to 8 h for the basal root zones.

These data emphasised the role of the apical root zones in acquiring NO_3^- from soil solution, and was consistent with the role played by root tips (Sorgonà and Cacco 2002) and highly branched root systems (dichotomous root topology) in NO_3^- induction (Sorgonà et al. 2005) previously demonstrated in citrus rootstock.

Spatial and temporal variation of H^+-ATPase protein abundance and root structure

Two aspects strictly concerning the NO_3^- uptake were further investigated along the tap root axis: (1) the anatomical barriers, such as suberisation of epidermal and exodermal cells, which could interfere with ion uptake (for a review see Hose et al. 2001); and (2) the variation of PM H^+-ATPase activity, an enzyme closely involved in NO_3^- uptake (Santi et al. 1995, 2003).

The present study indirectly demonstrated that the suberin incrustations of the hypodermal cells of citrus root dramatically decreased the surface area for NO_3^- uptake, which is confined to epidermal cells. Furthermore, since the thickened suberised exodermis was strictly close to the root apex, there was a similar surface area available for NO_3^- uptake along the citrus tap root. Hence, the homogeneous pattern of the NNUR along the citrus tap root could be due to the similar surface area of exposure to the external NO_3^- among the root zones. The reduction of the plasmalemma surface area for ion uptake by the exodermis was demonstrated by Kamula et al. (1994), and Colmer and Bloom (1998) suggested that NO_3^- uptake was limited by the exodermis in the basal root zones of maize.

However, this anatomical barrier did not justify the temporal variation of NO_3^- uptake characterised in each root region by the full induction phase at 24 h of exposure to external NO_3^-. Considering the central role played by H^+-ATPase in NO_3^- uptake as already demonstrated in whole roots of maize by Santi et al. (1995, 2003) and the temporal variation of the H^+ flux along the root axes (Shabala and Knowles 2002; Shabala 2003; Hayashi et al. 2005), the spatial–temporal variation of protein abundance was investigated. The results indicated that: (1) the PM H^+-ATPase protein was particularly concentrated in the PM of endodermis and vascular tissues; (2) the exposure to 100 μM NO_3^- increased the protein abundance in all root regions compared to the control (0 μM NO_3^-) and the increase was more conspicuous in the apical root segments

compared with basal segments, probably due to more densely packed cells; and (3) the immunostain increased with the time of NO_3^- exposure. These results suggested that the temporal pattern of NO_3^- uptake could be strictly correlated with increased H^+-ATPase abundance. These data confirmed the close link between NO_3^- and H^+ flux in root regions of citrus seedlings, as already demonstrated in whole root systems of other woody species (Garnett et al. 2003).

Conclusion

The reported data support the conclusions that, in terms of spatial distribution, the pattern of NO_3^- uptake did not vary along the citrus tap root axes and the presence of a uniform suberin incrustation of hypodermal cell layers could be responsible for this unchanged pattern of NO_3^- absorption. Conversely, in terms of temporal evolution, the NO_3^- uptake increased with time of exposure to external NO_3^- and the apical root segments had an earlier maximum induction than basal segments. The H^+-ATPase activity could be strictly correlated with this temporal pattern of NO_3^- uptake.

The 'potential' NO_3^- uptake capacity of the root segments evaluated by V_{max} and K_m, also confirmed the spatial uniformity and temporal heterogeneity of the NO_3^- uptake patterns along citrus tap root axes.

In summary, the apical root zones could be considered a plant evolutionary feature to deal with a highly mobile and heterogeneously distributed soil resource, such as NO_3^-.

References

Aslam M, Travis RL, Huffaker RC (1994) Stimulation of nitrate and nitrite efflux by ammonium in barley (Hordeum vulgare L.) seedlings. Plant Physiol 106:1293–1301

Behl R, Tischner R, Raschke K (1988) Induction of a high-capacity nitrate uptake mechanism in barley roots prompted by nitrate uptake through a constitutive low-capacity mechanism. Planta 176:235–240

Bloom AJ, Caldwell RM (1988) Root excision decreases nutrient absorption and gas fluxes. Plant Physiol 87:794–796

Caldwell MM (1994) Exploiting nutrients in fertile soil microsites. In: Caldwell MM, Pearcy RW (eds) Exploitation of environmental heterogeneity by plants. Academic Press, San Diego, pp 325–347

Cerezo M, Garcia-Augustin P, Serna MD, Primo-Millo E (1997) Kinetics of nitrate uptake by Citrus seedlings and inhibitory effects of salinity. Plant Sci 126:105–112

Colmer TD, Bloom AJ (1998) A comparison of NH_4^+ and NO_3^- net fluxes along root of rice and maize. Plant Cell Environ 21:240–246

Cruz C, Lips SH, Martins-Loucao MA (1995) Uptake regions of inorganic nitrogen in roots of carob seedlings. Physiol Plant 95:167–175

De Simone O, Haase K, Müller E, Junk WJ, Hartmann K, Schreiber L, Schmidt W (2003) Apoplasmic barriers and oxygen transport properties of hypodermal cell walls in roots from four amazonian tree species. Plant Physiol 132:206–217

Deane-Drummond CE, Glass ADM (1983) Short term studies of nitrate uptake into barley plants (Hordeum vulgare L cv Betzes) using ion specific electrodes and 36ClO3–l. Control of net uptake by NO_3^- efflux. Plant Physiol 7:100–104

Dell'Orto M, Pirovano L, Villalba JM, Gonzales-Reys JA (2002) Localization of the plasma membrane H^+-ATPase in Fe-deficient cucumber roots by immunodetection. Plant Soil 241:11–17

Engels C, Neumann G, Gahoonia TS, George E, Schenk M (2000) Assessing the ability of roots for nutrient acquisition. In: Smit AL, Bengough AG, Engels C, van Noordwijk M, Pellerin S, van de Geijn SC (eds) Root methods: a handbook. Springer, Berlin, pp 403–460

Forde BG (2000) Nitrate transporters in plants: structure, function and regulation. Biochim Biophys Acta 1465:219–235

Garnett TP, Shabala SN, Smethurst PJ, Newman IA (2001) Simultaneous measurement of ammonium, nitrate and proton fluxes along the length of eucalypt roots. Plant Soil 236:55–62

Garnett TP, Shabala SN, Smethurst PJ, Newman IA (2003) Kinetics of ammonium and nitrate uptake by eucalypt roots and associated proton fluxes measured using ion selective microelectrodes. Funct Plant Biol 30:1165–1176

Gobert A, Plassard C (2002) Differential NO_3^- dependent patterns of NO_3^- uptake in Pinus pinaster, Rhizopogon roseolus and their ectomycorrhizal association. New Phytol 154:509–516

Hawkins BJ, Boukcim H, Plassard C (2008) A comparison of ammonium, nitrate and proton net fluxes along seedling roots of Douglas-fir and lodgepole pine grown and measured with different inorganic nitrogen sources. Plant Cell Environ 31:278–287

Hayashi Y, Tanoi K, Nishiyama H, Nakanishi TM (2005) Rhizosphere pH profile of rice plant influenced by Al treatment. Soil Sci Plant Nutr 51:729–731

Henriksen GH, Raman DR, Walzer LP, Spanswick RM (1992) Measurement of net fluxes of ammonium and nitrate at the surface of barley roots using ion-selective microelectrodes II. Patterns of uptake along the root axis and evaluation of the microelectrode flux estimation technique. Plant Physiol 99:734–747

Holobrada M (1977) Changes in sulphate uptake and accumulation along the primary root during tissue differentiation. Biol Plant 19:331–337

Hose E, Clarkson DT, Steudle E, Schreiber L, Hartug W (2001) The exodermis: a variable apoplastic barrier. J Exp Bot 52:2245–2264

Imsande J, Touraine B (1994) N demand and the regulation of nitrate uptake. Plant Physiol 105:3–7

Kamula SA, Peterson CA, Mayfield CI (1994) The plasmalemma surface area exposed to the soil solution is markedly reduced by maturation of the exodermis and death of the epidermis in onion roots. Plant Cell Environ 17:1183–1193

Kronzucker HJ, Siddiqi MY, Glass DM (1995) Kinetics of NO_3^- influx in spruce. Plant Physiol 109:319–326

Lazof DB, Rufty TW, Redinbaugh MG (1992) Localization of nitrate absorption and translocation within morphological regions of the corn root. Plant Physiol 100:1251–1258

Lulai EC, Morgan WC (1992) Histochemical probing of potato periderm with neutral red: a sensitive cytofluorochrome for the hydrophobic domain of suberin. Biotech Histochem 67:185–195

Mancuso S, Boselli M (2002) Characterisation of the oxygen fluxes in the division, elongation and mature zones of Vitis roots: influence of oxygen availability. Planta 214:767–774

Mengel K, Kirby EA (1980) Potassium in crop production. Adv Agron 33:59–110

Monte R, Cesco S, Locci G, Pinton R, Varanini Z (2005) Induction of nitrate uptake and PM H$^+$-ATPase activity along the root axis of maize seedlings. In: Li CJ, Zhang FS, Doberman A, Hinsinger P, Li XL (eds) Plant nutrition for food security human health and environmental protection. Tsinghua University Press, Beijing, pp 220–221

Peterson CA (1988) Exodermal Casparian bands: their significance for ion uptake by roots. Physiol Plant 72:204–208

Plassard C, Guérin-Laguette A, Véry A, Casarin V, Thibaud JB (2002) Local measurements of nitrate and potassium fluxes along roots of maritime pine. Effects of ectomycorrhizal symbiosis. Plant Cell Environ 25:75–84

Press WH, Teukosky SA, Wetterling WT, Flannery BP (1992) Numerical recipes in C. The art of scientific computing. Cambridge University Press, Cambridge

Reidenbach G, Horst WJ (1997) Nitrate-uptake capacity of different root zones of Zea mays (L.) in vitro and in situ. In: Ando T, Fujita K, Mae T, Matsumoto H, Mori S, Sekiya J (eds) Plant nutrition-for sustainable food production and environment. Kluwer, Dordrecht, pp 663–668

Rubinigg M, Stulen I, Elzenga JTM, Colmer TD (2002) Spatial patterns of radial oxygen loss and nitrate net flux along adventitious roots of rice raised in aerated or stagnant solution. Funct Plant Biol 29:1475–1481

Rubio G, Sorgonà A, Lynch JP (2004) Spatial mapping of phosphorus influx in bean root systems using digital autoradiography. J Exp Bot 55:2269–2280

Santi S, Locci G, Pinton R, Cesco S, Varanini Z (1995) Plasma membrane H$^+$-ATPase in maize roots induced for NO$_3^-$ uptake. Plant Physiol 109:1277–1283

Santi S, Locci G, Monte R, Pinton R, Varanini Z (2003) Induction of nitrate uptake in maize roots: expression of a putative high-affinity nitrate transporter and plasma membrane H$^+$-ATPase isoforms. J Exp Bot 389:1851–1864

Shabala S (2003) Physiological implications of ultradian oscillations in plant roots. Plant Soil 255:217–226

Shabala S, Knowles A (2002) Rhythmic patterns of nutrient acquisition by wheat roots. Funct Plant Biol 29:595–605

Siddiqi MY, Glass ADM, Ruth TJ, Fernando M (1989) Studies of the regulation of nitrate influx by barley seedlings using ^{13}NO$_3^-$. Plant Physiol 90:806–813

Siebrecht S, Mack G, Tischner R (1995) Function and contribution of the root tip in the induction of NO$_3^-$ uptake along the barley root axis. J Exp Bot 46:1669–1676

Sorgonà A, Cacco G (2002) Linking the physiological parameters of nitrate uptake with root morphology and topology in wheat (Triticum durum Desf.) and in citrus rootstock (Citrus volkameriana Ten & Pasq). Can J Bot 80:494–503

Sorgonà A, Abenavoli MR, Cacco G (2005) A comparative study between two citrus rootstocks: effect of nitrate on the root morpho-topology and net nitrate uptake. Plant Soil 270:257–267

Waisel Y, Eshel A (2002) Functional diversity of various constituents of a single root system. In: Waisel Y, Eshel A, Kafkafi U (eds) Plant roots. The hidden half. Marcel Dekker, New York, pp 157–174

Walker RR, Sedgley M, Blesing MA, Douglas TJ (1984) Anatomy, ultrastructure and assimilate concentrations of roots of citrus genotypes differing in ability for salt exclusion. J Exp Bot 35:1481–1494